Inverse Problems **16** (2000) 1043–1052. Printed in the UK PII: S0266-5611(00)12515-8

Numerical method for finding the convex hull of an inclusion in conductivity from boundary measurements

M Ikehata† and S Siltanen‡§

† Department of Mathematics, Faculty of Engineering, Gunma University, Kiryu 376, Japan
‡ Instrumentarium Corp. Imaging Division, PO Box 20, FIN-04301 Tuusula, Finland

Received 13 March 2000, in final form 12 May 2000

Abstract. We consider the 2D inverse conductivity problem for conductivities of the form $\gamma = 1 + \chi_D h$ defined in a bounded domain $\Omega \subset \mathbb{R}^2$ with C^∞ boundary $\partial\Omega$. Here $D \subset \Omega$ and $h \in L^\infty(D)$ are such that γ has a jump along ∂D. It was shown by Ikehata (Ikehata M *J. Inverse and Ill-Posed Problems* at press) that the Dirichlet–Neumann map determines the indicator function $I_\omega(\tau, t)$ that can be used to find the convex hull of D. In this paper we find numerically the indicator function for examples with constant h and recover the convex hull of D.

1. Introduction

Let $\Omega \subset \mathbb{R}^2$ be a bounded, simply connected C^∞ domain and

$$\gamma = 1 + \chi_D h : \Omega \to \mathbb{R}^+. \tag{1}$$

Here $D \subset \Omega$ and $h \in L^\infty(D)$ is such that γ is bounded away from zero and has a jump along ∂D in a sense defined in section 2. We do not make assumptions on the openness or connectedness of D.

We define the Dirichlet–Neumann map corresponding to γ by

$$\Lambda_\gamma : H^{1/2}(\partial\Omega) \to H^{-1/2}(\partial\Omega), \qquad \langle \Lambda_\gamma f, g \rangle = \int_\Omega \gamma \nabla u \cdot \nabla v, \tag{2}$$

where v is any $H^1(\Omega)$ function with trace g on the boundary and u is the unique $H^1(\Omega)$ solution of the Dirichlet problem

$$\begin{aligned} &\nabla \cdot \gamma \nabla u = 0 \text{ in } \Omega, \\ &u = f \text{ on } \partial\Omega. \end{aligned} \tag{3}$$

The inverse conductivity problem of Calderón [3] is to decide whether γ is uniquely determined by Λ_γ and, if so, reconstruct γ from knowledge of Λ_γ. This has applications in geophysics, nondestructive testing and medical imaging. The map Λ_γ represents static electrical measurements on the boundary of an unknown physical body.

The study of Calderón's problem may be divided into three categories. The first one is the uniqueness and stability problem. For uniqueness results, see [4, 14, 15, 18, 23] and references therein. For the stability problem there are only two results [1, 16]. The second step is to find a formula which directly connects γ or its discontinuity with Λ_γ. For this problem see [9–11, 17, 18, 22]. Note that in [12] a formula which directly connects a convex

§ To whom correspondence should be addressed.

0266-5611/00/041043+10$30.00 © 2000 IOP Publishing Ltd

polygonal domain, where γ vanishes, with $\Lambda_\gamma f$ for a single f is given. The third step is to give a practical reconstruction algorithm. Many such algorithms have been suggested, most relying on linearization or iterative minimization of a cost functional; for references see [6], but see also [5]. Reconstruction algorithms based on the nonlinear structure of the problem are described in [19, 20]. At present there is no completely satisfactory algorithm and thus it is of interest to find methods giving even partial answers to Calderóns question.

In this paper we implement the following numerical algorithm based on [8]. We define the support function of $D \subset \mathbb{R}^2$ with respect to any direction $\omega \in S^1$ by

$$h_D(\omega) := \sup_{x \in D} x \cdot \omega. \tag{4}$$

(Note that h_D is unrelated to the function h in (1).) Let $\omega^\perp$ be ω rotated counterclockwise by angle $\pi/2$; then $\omega \cdot \omega^\perp = 0$. For each $\tau > 0$ set

$$f_\omega(x; \tau) := \mathrm{e}^{\tau x \cdot \omega + \mathrm{i}\tau x \cdot \omega^\perp}, \qquad x \in \partial\Omega. \tag{5}$$

The indicator function $I_\omega(\tau)$ is defined by

$$I_\omega(\tau) := \langle (\Lambda_\gamma - \Lambda_1)\overline{f_\omega(\cdot; \tau)}, f_\omega(\cdot; \tau)\rangle. \tag{6}$$

We will prove in section 2 that as a function of τ, $\log|I_\omega(\tau)|$ is asymptotically linear when $\tau \to \infty$ and the slope can be used to approximate $h_D(\omega)$. In section 3 we derive practical formulae for the indicator function corresponding to certain conductivities. In section 4 we check numerically that reasonably accurate knowledge of $I_\omega(\tau)$ can be used to determine the convex hull of inclusions.

Strictly speaking, we do not solve numerically any inverse problem of the type: *given* Λ_γ, *find properties of* γ. To specify the relevance of our results we separate out the following two questions:

(a) Given numerical values of a function relating Λ_γ with properties of γ (such as $I_\omega(\tau)$), how do we extract computationally knowledge about γ?
(b) How do we compute $I_\omega(\tau)$ from practical measurements done with a finite number of electrodes and finite precision?

The motivation behind this separation is the fact that we are never, in practice, given the Dirichlet–Neumann (or Neumann–Dirichlet) map, although mathematically it is convenient to work with it. In this paper we compute $I_\omega(\tau)$ explicitly for a class of discontinuous conductivities and recover numerically the convex hull of the inclusion set D. These results answer question (a) and provide test material for studying (b). We do not discuss question (b) here; see [13, 21] for definitions of realistic electrode models and results on their relation to continuous boundary data.

Remark. While preparing the manuscript of this paper we received a preprint [2] written by Brühl and Hanke. They also undertook a numerical implementation of the method proposed in [8]. In contrast to us, they used synthetic data from a finite element simulation of the forward problem.

2. Description of the method

In this section, we summarize the method presented in [8]. For $\omega \in S^1$ and $\delta > 0$, we define

$$D_\omega(\delta) := \{x \in D|, h_D(\omega) - \delta < x \cdot \omega \leqslant h_D(\omega)\}$$

(see figure 1). We introduce two concepts related to γ and D.

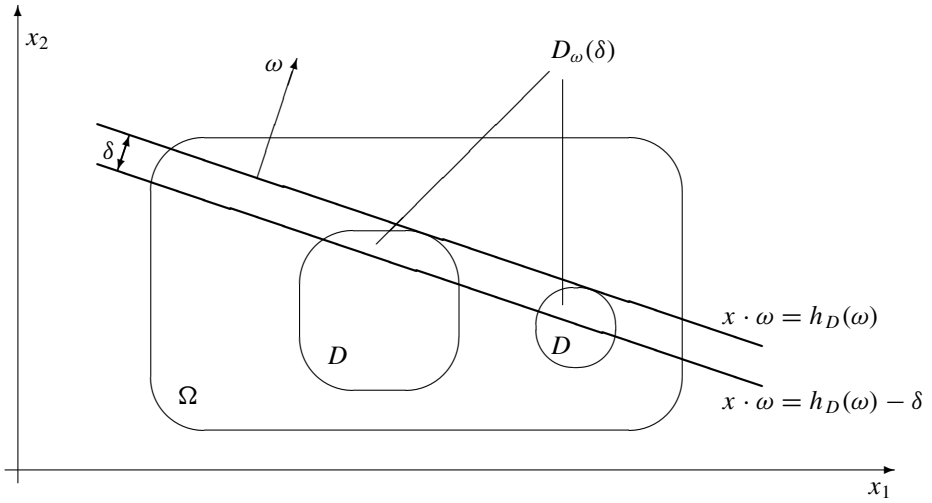

Figure 1. Illustration of h_D and $D_\omega(\delta)$ with D consisting of two disjoint components.

Definition 2.1. *The conductivity $\gamma = 1 + \chi_D h$ satisfies the jump condition if, for each $\omega \in S^1$, there exist positive constants C_ω and δ_ω such that*

$$h(x) \geqslant C_\omega \qquad \text{for almost all} \quad x \in D_\omega(\delta_\omega), \qquad \text{or}$$
$$-h(x) \geqslant C_\omega \qquad \text{for almost all} \quad x \in D_\omega(\delta_\omega).$$

Definition 2.2. *The subset $D \subset \Omega$ is regular if for each $\omega \in S^1$, there exist positive constants M_ω, ϵ_ω and $p \in [0, 1]$ such that*

$$\mu_1(\{x \in D | x \cdot \omega = h_D(\omega) - s\}) \geqslant M_\omega s^p, \qquad \forall s \in]0, \epsilon_\omega[$$

where μ_1 denotes the one-dimensional Lebesgue measure.

For example, if D is open and ∂D is Lipschitz, then D is regular. This is described in [8]. In addition, if $h \in C^0(\overline{D})$ and satisfies $h(a) > 0$ for all $a \in \partial D$ or $h(a) < 0$ for all $a \in \partial D$, γ satisfies the jump condition.

For each $(\tau, t) \in \mathbb{R}^+ \times \mathbb{R}$ and $\omega \in S^1$ set

$$f_\omega(x; \tau, t) := \mathrm{e}^{\tau(x \cdot \omega - t) + \mathrm{i}\tau x \cdot \omega^\perp}, \qquad x \in \partial\Omega. \tag{7}$$

The indicator function $I_\omega(\tau, t)$ is defined by

$$I_\omega(\tau, t) := \langle (\Lambda_\gamma - \Lambda_1)\overline{f_\omega(\cdot; \tau, t)}, f_\omega(\cdot; \tau, t) \rangle. \tag{8}$$

Proposition 2.1. *Assume that γ satisfies the jump condition and D is regular. For each $\omega \in S^1$, the set of all t that satisfies $\lim_{\tau \longrightarrow \infty} |I_\omega(\tau, t)| = 0$ coincides with the interval $]h_D(\omega), \infty[$.*

Proof. (Outline only, for details see theorem 2.1 of [8].) From the jump condition for γ and regularity on D we see that, for each ω, there exist positive constants C_1 and C_2 such that for $\tau > C_1$,

$$C_2 \tau^{1-p} \leqslant |I_\omega(\tau, h_D(\omega))| \leqslant C_2^{-1} \tau^2. \tag{9}$$

Since

$$I_\omega(\tau, t) = \mathrm{e}^{2\tau(h_D(\omega) - t)} I_\omega(\tau, h_D(\omega)), \qquad \forall t$$

we obtain

$$C_2\tau^{1-p}\mathrm{e}^{2\tau(h_D(\omega)-t)} \leqslant |I_\omega(\tau,t)| \leqslant C_2^{-1}\tau^2\mathrm{e}^{2\tau(h_D(\omega)-t)} \tag{10}$$

and this thus yields the desired conclusion. □

The next formula is not explicitly written in [8], however, the proof is an easy consequence of (10).

Theorem 2.1. *Under the same assumption on γ and D, for each t we have the formula*

$$h_D(\omega) - t = \lim_{\tau\longrightarrow\infty} \frac{\log|I_\omega(\tau,t)|}{2\tau}. \tag{11}$$

Formula (11) shows that to determine $h_D(\omega)$, only one value of t is needed. We will set $t = 0$ and the origin of the formulae (5) and (6) becomes clear:

$$f_\omega(x;\tau) = f_\omega(x;\tau,0), \qquad I_\omega(\tau) = I_\omega(\tau,0).$$

Our algorithm is based on the formula

$$h_D(\omega) = \lim_{\tau\longrightarrow\infty} \frac{\log|I_\omega(\tau)|}{2\tau}, \tag{12}$$

where the quotient on the right-hand side is approximately constant for large τ.

We note that the method can be used also in the case of nonconstant background conductivity, that is, $\gamma = \gamma_0 + h\chi_D$. Then one has to replace the functions $f_\omega(x;\tau,t)$ by the exponentially growing solutions corresponding to γ_0 as introduced in [18, 23]. See [10] for the treatment of a similar problem. Computation of these functions in the case $\gamma_0 \in C^2(\Omega)$ and $\gamma_0 \equiv 1$ near $\partial\Omega$ is described in [19].

3. Computational formulae for $I_\omega(\tau)$

In testing algorithms for electrical impedance tomography, a central problem is the accurate computation of Dirichlet–Neumann maps for given conductivities. It is well known that for piecewise constant radial conductivities this is possible to do in closed form. In this case the indicator function can be written as a sum with precisely known terms. Using suitable pullbacks we will also derive such a formula for a class of nonradial conductivities.

Throughout the rest of this paper, let Ω be the unit disc. We identify a point $x = (x_1, x_2)$ with the complex number $x_1 + \mathrm{i}x_2$. As pointed out in [22], the functions x^n, $n = 0, \pm1, \pm2, \ldots$ are eigenfunctions for Λ_γ if γ is radial. The following proposition gives a practical formula for the indicator function for a class of radial conductivities.

Proposition 3.1. *Let $\gamma : \Omega \to \mathbb{R}$ be the rotationally symmetric function*

$$\gamma(x) = \begin{cases} c & for \quad 0 \leqslant |x| \leqslant \rho, \\ 1 & for \quad \rho < |x| < 1, \end{cases} \qquad \text{where} \quad 0 < \rho < 1, \qquad 0 < c. \tag{13}$$

Then $\Lambda_\gamma x^n = \lambda_n x^n$ with

$$\lambda_n = |n| - 2|n|\left(\frac{(1-c)\rho^{2|n|}}{1+c+(1-c)\rho^{2|n|}}\right) \tag{14}$$

and the indicator function corresponding to γ can be computed as

$$I_\omega(\tau) = 2\pi\sum_{n=1}^{\infty}\frac{(\lambda_n - n)\tau^{2n}}{(n!)^2}. \tag{15}$$

Proof. Formula (14) can be found, e.g., in [1, 2, 7, 19].

Formula (15) appears in [2] but for convenience we present a short proof. Fix $\omega = \omega_1 + \mathrm{i}\omega_2 \in S^1$; then $\omega^\perp = -\omega_2 + \mathrm{i}\omega_1$. Let $\tau > 0$. Using the complex notation $x \cdot \tau\omega + \mathrm{i}x \cdot \tau\omega^\perp = x\tau\overline{\omega}$ we know $f_\omega(x;\tau) = \sum_{n=0}^\infty \tau^n \overline{\omega}^n x^n/n!$. Thus (15) follows from

$$I_\omega(\tau) = \int_{|x|=1} \sum_{m=0}^\infty \frac{\tau^m \omega^m}{m!} x^{-m} \sum_{n=0}^\infty \frac{\tau^n \overline{\omega}^n}{n!} (\lambda_n - |n|) x^n |\,\mathrm{d}x|.$$

□

We note that the usefulness of formula (15) comes from the explicit expression for the difference $\lambda_n - |n|$ given by (14). Note also that (15) can be generalized for piecewise constant radial conductivities and further, approximately, for radial continuous conductivities [19].

We also need examples without rotational symmetry. To describe a suitable class of examples we consider pullbacks of radial conductivities by a holomorphic function Ψ that is one-to-one. Note that Ψ gives a conformal mapping between Ω and $\Psi(\Omega)$.

Theorem 3.1. *Let γ be given by (13) and let Ψ be a holomorphic injection defined on a neighbourhood of $\overline{\Omega}$; then $\tilde{\Omega} := \Psi(\Omega)$ is a domain and Ψ has the expansion*

$$\Psi(x) = \sum_{n=0}^\infty b_n x^n, \qquad x \in \Omega. \tag{16}$$

The indicator function corresponding to the conductivity $\tilde{\gamma} := \gamma \circ \Psi^{-1}$ on $\tilde{\Omega}$ can be computed from

$$I_\omega(\tau) = 2\pi \sum_{n=1}^\infty |a_n(\tau\overline{\omega})|^2 (\lambda_n - n), \tag{17}$$

where the functions $a_n(x)$ are given for complex $x = x_1 + \mathrm{i}x_2$ recursively by

$$a_0(x) = \mathrm{e}^{b_0 x}, \qquad a_n(x) = \frac{x}{n} \sum_{l=0}^{n-1} (n-l) b_{n-l} a_l(x), \qquad n = 1, 2, 3, \ldots. \tag{18}$$

Proof. Let $\varphi \in H^1(\Omega)$ and set $\tilde{\varphi}(y) = \varphi(\Psi^{-1}(y))$. A change of variables yields

$$\int_{\tilde{\Omega}} \tilde{\gamma} \nabla\tilde{u} \cdot \nabla\tilde{\varphi}\,\mathrm{d}y = \int_\Omega \gamma (\Psi'(x)^{-1})^T \nabla u \cdot (\Psi'(x)^{-1})^T \nabla\varphi |\det \Psi'(x)|\,\mathrm{d}x.$$

Since Ψ is holomorphic, it follows from the Cauchy–Riemann condition that

$$\Psi'(x)^{-1}(\Psi'(x)^{-1})^T = \frac{1}{\det \Psi'(x)} \begin{bmatrix} 1 & 0 \\ 0 & 1 \end{bmatrix}.$$

Now $\det \Psi'(x) > 0$ gives $\int_{\tilde{\Omega}} \tilde{\gamma} \nabla\tilde{u} \cdot \nabla\tilde{\varphi}\,\mathrm{d}y = \int_\Omega \gamma \nabla u \cdot \nabla\varphi\,\mathrm{d}x$. This thus yields that u is a weak solution to the equation $\nabla \cdot \gamma \nabla u = 0$ in Ω, if and only if $\tilde{u}(y) = u(\Psi^{-1}(y))$ is a weak solution to the equation $\nabla \cdot \tilde{\gamma} \nabla\tilde{u} = 0$ in $\tilde{\Omega}$. Moreover we have

$$\langle \Lambda_{\tilde{\gamma}}(\mathrm{e}^{\tau y\overline{\omega}}|_{\partial\tilde{\Omega}}), \mathrm{e}^{\tau\overline{y}\omega}|_{\partial\tilde{\Omega}} \rangle = \langle \Lambda_\gamma(\mathrm{e}^{\tau\Psi(x)\overline{\omega}}|_{\partial\Omega}), \mathrm{e}^{\tau\overline{\Psi(x)}\omega}|_{\partial\Omega} \rangle.$$

The same obviously holds for Λ_1, and by linearity

$$I_\omega(\tau) = \langle (\Lambda_\gamma - \Lambda_1)(\mathrm{e}^{\tau\Psi(x)\overline{\omega}}|_{\partial\Omega}), \mathrm{e}^{\tau\overline{\Psi(x)}\omega}|_{\partial\Omega} \rangle. \tag{19}$$

Here one may write

$$\mathrm{e}^{\tau\Psi(x)\overline{\omega}} = \sum_{n=0}^\infty a_n x^n, \qquad x \in \Omega.$$

Differentiating both sides with respect to x one knows that $a_n = a_n(\tau\overline{\omega})$ given by (18). Now (17) is clear. □

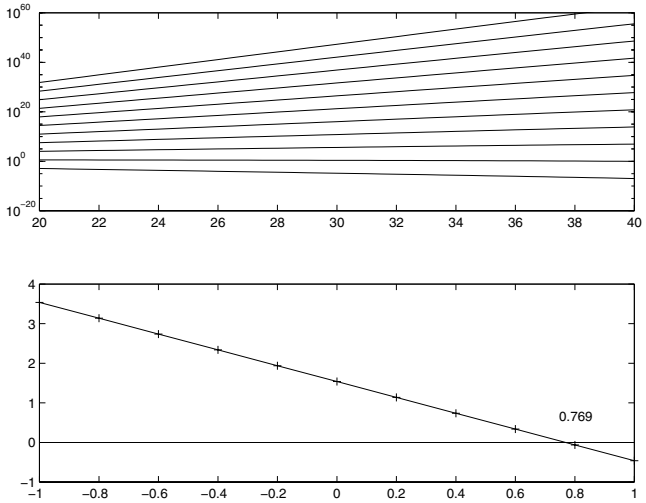

Figure 2. Upper plot: the functions $\log|I_\omega(\tau, t)|$ corresponding to γ_1 in the range $\tau \in [20, 40]$ for $t = -1, -0.8, \ldots, 0.8, 1$. Here the number of eigenvalues was 32 and the parameters of γ_1 were $\rho = 0.75$, $c = 10$. Lower plot: slopes of the approximately linear functions of the upper plot as a function of t.

4. Numerical examples

In this section, we define explicitly conductivities for which we can compute indicator functions numerically using the formulae derived in section 3. Having $I_\omega(\tau)$ computed for a fixed direction $\omega \in S^1$ and a collection of τ values, we can numerically evaluate the support function $h_D(\omega)$ of the set D. This determines a half-space where D has to lie, and we indicate this by drawing the line $\{x \in \mathbb{R}^2 | x \cdot \omega = h_D(\omega)\}$. These lines, corresponding to a collection $\{\omega\} \subset S^1$, outline the convex hull of D; see figures 5 and 7.

Computation times for all the examples below are less than 30 s with a PC equipped with Pentium II 250 MHz processor and Matlab.

4.1. Radial examples

We consider in this section conductivities satisfying $\gamma(x) = \gamma(|x|)$. Note that due to symmetry it is enough to compute $I_\omega(\tau)$ for only one $\omega \in S^1$.

The sum in (15) must be truncated. Thus, we can expect that our calculation becomes useless for τ values larger than some τ_1. We estimate τ_1 by repeating the computation with different amounts of eigenvalues and checking if the computed functions change. Also, the powers of τ in the inequality (10) suggest that the behaviour of $\log|I_\omega(\tau)|$ is only asymptotically linear for large τ. Hence, we should work in an interval $\tau \in [\tau_0, \tau_1]$ with some $\tau_0 > 0$.

We now define γ_1 by (13) with $c = 10$ and $\rho = \frac{3}{4}$. We fix $\omega = (0, 1) \in S^1$ and take the number of eigenvalues in (15) to be 32. Let us examine formula (12) numerically: for each t in the collection $t \in \{-1, -0.8, \ldots, 1\}$ we make a least-square fit of a first-order τ-polynomial to find the slopes of the functions $\log|I_\omega(\cdot, t)|$. Here $\tau \in [20, 40]$; see figure 2 for plots of the functions $\log|I_\omega(\tau, t)|$ and their slopes. Note the linearity of the lower function predicted by formula (12). Thus, any choice of t leads to the reconstruction $\rho = 0.769$; from now on we will set $t = 0$ and use formula (12).

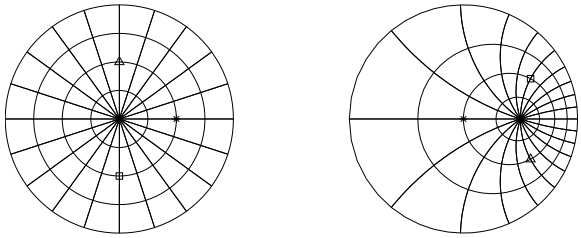

Figure 3. Action of the linear fractional transformation Ψ of section 4.2. The images of three points are marked for clarity. Note that $\Psi(\Omega) = \Omega$ and that $\Psi^{-1} = \Psi$.

We note that the above results are identical (within six digits accuracy) with the choices $c = 1.2$ and $c = 100$.

As our second example, we repeat the above method with γ_2 given by (13), where $c = \frac{1}{10}$ and $\rho = \frac{1}{4}$. The reconstruction gives $\rho = 0.276$, and computing with $c = 0.9$ does not change the result.

4.2. Nonradial examples with disc inclusions

We choose a special holomorphic map Ψ. We identify $\mathbb{C} = \mathbb{R}^2$ and define Ψ in a neighbourhood of the closed unit disc $\overline{\Omega}$ by

$$\Psi(x) := \frac{x - \frac{1}{2}}{\frac{x}{2} - 1}, \qquad x = x_1 + \mathrm{i}x_2; \tag{20}$$

see figure 3. Then $\Psi \in \{(x - a)(\overline{a}x - 1)^{-1}\mathrm{e}^{\mathrm{i}\alpha} | a \in \mathbb{C}, |a| < 1, \alpha \in \mathbb{R}\}$, the well-known class of conformal bijections $\overline{\Omega} \to \overline{\Omega}$ mapping $\partial\Omega$ onto itself. Therefore $\tilde{\Omega} = \Psi(\Omega) = \Omega$. Moreover, Ψ is a Möbius transformation and maps circles in the interior of Ω to other such circles. We write

$$\Psi(x) = \sum_{n=0}^{\infty} b_n x^n, \qquad b_0 = \tfrac{1}{2}, \qquad b_n = -\frac{3}{2^{n+1}}, \qquad n = 1, 2, 3, \ldots, \tag{21}$$

and we are ready to compute indicator functions with formulae (17) and (18).

Consider the conductivity $\tilde{\gamma}_1 = \gamma_1 \circ \Psi^{-1}$. It is easily computed that $\tilde{\gamma}_1(x) = 10$ for $x \in D$ and $\tilde{\gamma}_1 = 1$ otherwise, where D is the disc of radius $R = \frac{36}{55}$ centred at $(C, 0) \in \Omega$ with $C = \frac{14}{55}$. To estimate the validity domain of the truncated sum (17), we evaluate $I_{\omega_0}(\tau)$ with $\omega_0 = \exp(2\pi\mathrm{i}/3)$ numerically in the range $\tau \in [10, 100]$ for 32, 64 and 128 eigenvalues λ_n. The results suggest setting $\tau_0 = 10$, $\tau_1 = 20$ for computations with 32 eigenvalues; see figure 4. We perform the reconstruction for 31 directions with $\tau = 10, 11, \ldots, 20$, and compare the reconstructed values of h_D to the correct support function given by $h_D(\omega) = R - C\cos(\pi - \omega)$. The maximum relative error is 3%; see figure 5. The same computation with 128 eigenvalues and $\tau = 50, 55, \ldots, 80$ reduces the error to less than 1%.

We take as the second example the conductivity $\tilde{\gamma}_2 = \gamma_2 \circ \Psi^{-1}$. Now $\tilde{\gamma}_2(x) = \frac{1}{10}$ for x in the disc determined by $R = \frac{4}{21}$ and $C = \frac{10}{21}$, and $\tilde{\gamma}_2 = 1$ otherwise. Curiously, 32, 64 and 128 eigenvalues all give roughly the same function $I_\omega(\tau)$. Reconstructing h_D with 32 eigenvalues and $\tau = 40, 45, \ldots, 70$ yields an error of less than 7%; see figure 5. Performing the reconstruction with more eigenvalues does not improve the accuracy.

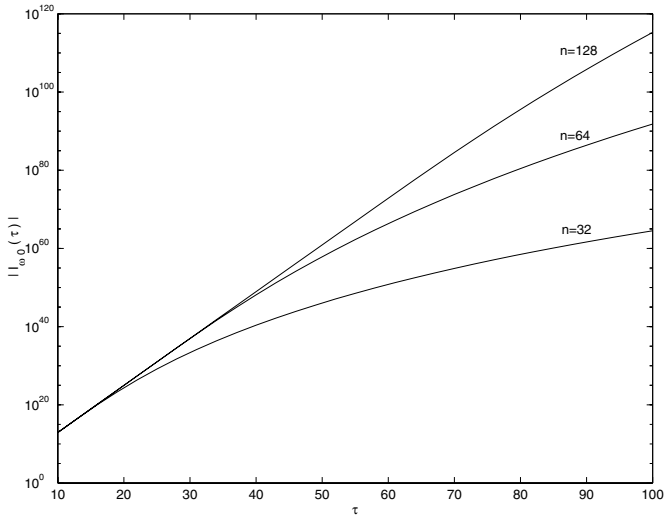

Figure 4. The function $|I_{\omega_0}(\tau)|$ corresponding to the conductivity $\tilde{\gamma}_1$ of section 4.2 evaluated approximately by truncating the sum (17) at $n = 32, 64$ and 128. Here $\omega_0 = e^{2\pi i/3}$. Note the logarithmic scale in the vertical axis.

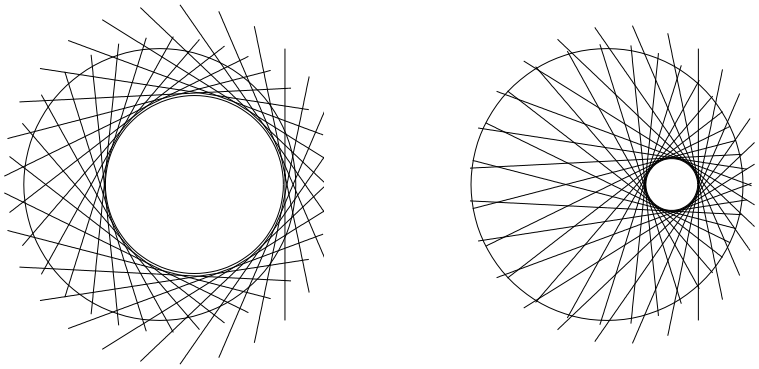

Figure 5. Left: the reconstruction of the jump of $\tilde{\gamma}_1$ of section 4.2 for 31 equispaced directions ω. Each line determines a half-space containing the inclusion D; this way the lines enclose the convex hull of D. Right: the same reconstruction for $\tilde{\gamma}_2$.

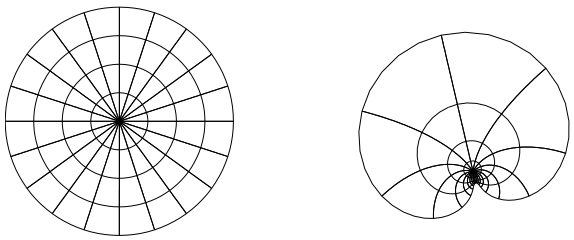

Figure 6. Action of the holomorphic map F of section 4.3. Note that $\tilde{\Omega} := F(\Omega) \neq \Omega$ in this case.

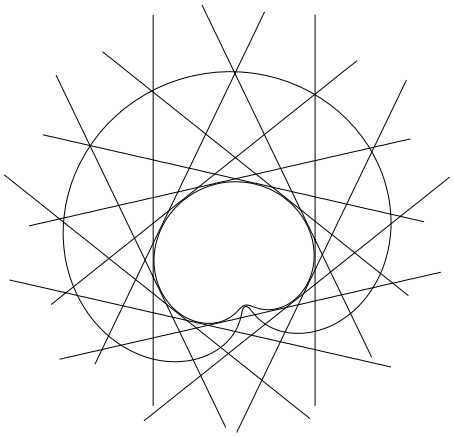

Figure 7. The reconstruction of the jump of $\tilde{\gamma}_3$ of section 4.3 for 14 equispaced directions ω.

4.3. A nonradial and nonconvex example

Here we choose as the holomorphic injection

$$F(x) = C\mathrm{e}^{Ax} + B, \qquad A = \tfrac{5}{2}, \qquad B = -\frac{\mathrm{i}}{2} + \frac{1}{10}, \qquad C = \frac{\mathrm{e}^{1.8\mathrm{i}}}{10};$$

see figure 6. This leads to the following form for coefficients (16):

$$b_0 = B + C, \qquad b_n = \frac{CA^n}{n!}, \qquad n = 1, 2, 3, \ldots.$$

We define $\tilde{\gamma}_3 = \gamma_1 \circ F^{-1}$, with γ_1 defined in section 4.1, and take $\rho = \frac{3}{4}$ and $c = 10$. Using 128 terms in the sum (17) produces the reconstruction shown in figure 7.

Acknowledgment

This research was supported by Grant-in-Aid for Scientific Research (Grant no 11640151), Ministry of Education, Science and Culture, Japan.

References

[1] Alessandrini G 1988 Stable determination of conductivity by boundary measurements *Applicable Analysis* **27** 153–72

[2] Brühl M and Hanke M 2000 Numerical implementation of two non-iterative methods for locating inclusions by impedance tomography *Inverse Problems* **16** 1029

[3] Calderón A P 1980 On an inverse boundary value problem *Seminar on Numerical Analysis and its Applications to Continuum Physics* (Rio de Janeiro: Soc. Brasileira de Matemàtica) pp 65–73

[4] Brown R M and Uhlmann G 1997 Uniqueness in the inverse conductivity problem for nonsmooth conductivities in two dimensions *Commun. Partial Diff. Eqns* **22** 1009–27

[5] Borcea L, Berryman J G and Papanicolaou G C 1999 Matching pursuit for imaging high-contrast impedance tomography *Inverse Problems* **15** 811–49

[6] Cheney M, Isaacson D and Newell J C 1999 Electrical impedance tomography *SIAM Rev.* **41** 85–101

[7] Gisser D G, Isaacson D and Newell J C 1990 Electric current tomography and eigenvalues *SIAM J. Appl. Math.* **50** 1623–34

[8] Ikehata M Reconstruction of the support function for inclusion from boundary measurements *J. Inverse and Ill-Posed Problems* at press
[9] Ikehata M 1998 Reconstruction of the shape of the inclusion by boundary measurements *Commun. Partial Diff. Eqns* **23** 1459–74
[10] Ikehata M 1999 How to draw a picture of an unknown inclusion from boundary measurements. Two mathematical inversion algorithms *J. Inverse and Ill-Posed Problems* **7** 255–71
[11] Ikehata M and Nakamura G 1999 Slicing of a three-dimensional object from boundary measurements *Inverse Problems* **15** 1243–53
[12] Ikehata M 1999 Enclosing a polygonal cavity in a two-dimensional bounded domain from Cauchy data *Inverse Problems* **15** 1231–41
[13] Isaacson D and Cheney M 1991 Effects of measurement precision and finite numbers of electrodes on linear impedance imaging algorithms *SIAM J. Appl. Math.* **51** 1705–31
[14] Isakov V 1998 *Inverse Problems for Partial Differential Equations* (Berlin: Springer)
[15] Kohn R V and Vogelius M 1985 Determining conductivity by boundary measurements II. Interior results *Commun. Pure Appl. Math.* **38** 643–67
[16] Liu L 1997 Stability estimates for the two-dimensional inverse conductivity problem *PhD Thesis* University of Rochester
[17] Nachman A I 1988 Reconstructions from boundary measurements *Annals of Mathematics* **128** 531–76
[18] Nachman A I 1996 Global uniqueness for a two-dimensional inverse boundary value problem *Annals of Mathematics* **143** 71–96
[19] Siltanen S, Mueller J and Isaacson D 2000 An implementation of the reconstruction algorithm of A Nachman for the 2D inverse conductivity problem *Inverse Problems* **16** 681–99
[20] Somersalo E, Cheney M, Isaacson D and Isaacson E 1991 Layer stripping: a direct numerical method for impedance imaging *Inverse Problems* **7** 899–926
[21] Somersalo E, Cheney M and Isaacson D 1992 Existence and uniqueness for electrode models for electric current computed tomography *SIAM J. Appl. Math.* **52** 1023–40
[22] Sylvester J 1992 A convergent layer stripping algorithm for the radially symmetric impedance tomography problem *Commun. Partial Diff. Eqns* **17** 1955–94
[23] Sylvester J and Uhlmann G 1987 A global uniqueness theorem for an inverse boundary value problem *Annals of Mathematics* **125** 153–69